HHS Public Access

Author manuscript

Med Image Comput Comput Assist Interv. Author manuscript; available in PMC 2016 October 01.

Published in final edited form as:

Med Image Comput Comput Assist Interv. 2015 October ; 9350: 263–271. doi: 10.1007/978-3-319-24571-3_32.

Mid-Space-Independent Symmetric Data Term for Pairwise Deformable Image Registration

Iman Aganj[1], **Juan Eugenio Iglesias**[2], **Martin Reuter**[1,3], **Mert Rory Sabuncu**[1,3], and **Bruce Fischl**[1,3]

[1] Athinoula A. Martinos Center for Biomedical Imaging, Radiology Department, Massachusetts General Hospital, Harvard Medical School, Boston, MA, USA

[2]Basque Center on Cognition, Brain and Language (BCBL), San Sebastian, Spain, e.iglesias@bcbl.eu

[3]Computer Science and Artificial Intelligence Laboratory, Massachusetts Institute of Technology, Cambridge, MA, USA

Abstract

Aligning a pair of images in a mid-space is a common approach to ensuring that deformable image registration is symmetric – that it does not depend on the arbitrary ordering of the input images. The results are, however, generally dependent on the choice of the mid-space. In particular, the set of possible solutions is typically affected by the constraints that are enforced on the two transformations (that deform the two images), which are to prevent the mid-space from drifting too far from the native image spaces. The use of an implicit atlas has been proposed to define the mid-space for pairwise registration. In this work, we show that by aligning the atlas to each image in the native image space, implicit-atlas-based pairwise registration can be made independent of the mid-space, thereby eliminating the need for anti-drift constraints. We derive a new symmetric cost function that only depends on a single transformation morphing one image to the other, and validate it through diffeomorphic registration experiments on brain magnetic resonance images.

1 Introduction

Image registration – i.e., computation of a set of dense spatial correspondences among images – is a central step in most population and longitudinal imaging studies. Since linear transformation is usually not sufficient to account for cross-subject variation and temporal changes in the anatomy, deformable image registration often becomes a necessary part of the analysis pipeline. In pairwise deformable registration, the choice of the reference space in which the two images are compared affects the registration, making the resulting deformation field dependent on this choice. When the native space of one of the input images (say, the first image) is chosen as the reference, the registration becomes *asymmetric*, meaning that reversing the order of the input images will produce different spatial correspondences [1-11]. Pairwise registration has been proposed to be symmetrized by minimizing the average of two cost functions, each using one input image as the

iman@nmr.mgh.harvard.edu, mreuter@nmr.mgh.harvard.edu, msabuncu@nmr.mgh.harvard.edu, fischl@nmr.mgh.harvard.edu

reference space [1-4], yet integrating the mismatch measure non-uniformly in the native space of the interpolated image [11].

In a different approach to achieve symmetry, both images are deformed and compared in a *mid-space*, thereby making registration invariant with respect to the ordering of the images [5-10]. Such approaches essentially minimize their cost functions with respect to *two* transformations T_1 and T_2 that take the two input images to the mid-space. However, without additional constraints, this increases the degrees of freedom of the problem twofold, compared to the end result of pairwise registration that is the *one* transformation, $T=T_2 \circ T_1^{-1}$, taking the second input image to the first. Furthermore, if the images are compared in the mid-space (that depends on T_1 and T_2), the optimization algorithm is given the liberty to update the mid-space so as to decrease the cost function without necessarily changing the final result T. For example, the algorithm can shrink the regions with mismatching image intensities to make the deformed images look more similar in the mid-space, without necessarily making them more similar in the two native spaces. To alleviate these issues, additional constraints are used to keep the mid-space "in between" the native spaces of the two images. These *anti-drift* constraints, which are different from those regularizing the transformations, define the mid-space. They typically either restrict the space of possible T_1 and T_2 (resulting in fewer degrees of freedom), or penalize those values of T_1 and T_2 that move the mid-space away from the native spaces. The most common such constraints, proposed in the mid-space registration and atlas construction literature, are restrictions on T_1 and T_2 to have opposite displacement [7, 8, 12-14] or velocity [9, 10, 15] fields. In large deformation models, geodesic averaging of the deformations has also been proposed, which preserves the properties of the transformations [5, 6, 16]. The choice of the anti-drift constraints may bias the registration algorithm towards favoring a particular set of transformations, thereby affecting the resulting T.

Unbiased *atlas* construction techniques, when applied to a pair of images, can constitute mid-space pairwise registration, since the images are both deformed to the atlas space (i.e., the mid-space) [10, 16, 17]. In such a case, given that the desired output of pairwise image registration is the deformation field, but not the auxiliary atlas, one can substitute the atlas in the cost function with an analytical expression of the two deformed images, leading to an implicit-atlas cost function that is minimized with respect to the deformations. To that end, it was initially proposed to compare the deformed images to the atlas in the abstract mid-space [16]. A better justified generative model, however, progresses from the atlas to the images and compares the deformed atlas to the images (i.e., in the native image spaces) [18, 19], computing the atlas as a weighted average of the images [18]. Taking advantage of this native-space atlas construction resolves the issue of susceptibility to shrinkage-type problems, leading to a proper implicit-atlas cost function for mid-space pairwise registration [10]. Nevertheless, the registration still remains a function of *two* transformations taking the images to a mathematically defined mid-space.

In this work, we point out for the first time the key fact that implicit-atlas pairwise registration is inherently independent of the mid-space. We show that the cost function only depends on the overall image-to-image transformation T, implying that the individual

image-to-atlas transformations T_1 and T_2 are redundant and unnecessary to keep, and that anti-drift constraints are indeed not needed. We derive a new cost function that, in contrast to the existing mid-space approaches, can be minimized directly with respect to T, with no anti-drift constraints. The proposed cost function is general and can be used with any transformation model, such as the displacement and velocity fields.

We describe our methodology in Section 2, experimentally evaluate our approach on brain magnetic resonance images in Section 3, and conclude the paper in Section 4.

2 Methods

2.1 Mid-Space Approach to Registration Symmetry

Let $I_1, I_2{:}\Omega \rightarrow \mathbb{R}$ be the two d -dimensional input images to be registered, where $\Omega \subseteq \mathbb{R}^d$. We want to compute the regular transformation T: $\Omega \rightarrow \Omega$ that deforms I_2 so as to make I_1 and $I_2 \bigcirc T$ most similar to each other; a task that is often done by minimizing a cost function with respect to T. The data term of the common sum of squared differences (SSD) cost function can be formulated for instance as $\|I_1 - I_2 \circ T\|_2^2$ or $\|I_1 \circ T^{-1} - I_2\|_2^2$. These two forms are not equivalent though, because the transformed image – which is different in each case – is integrated non-uniformly [1-4, 11], resulting in the registration asymmetry.

In a popular approach to derive a symmetric cost function, both images are deformed to a *mid-space* [5-10]. Consequently, these cost functions depend on two transformations, T_1, T_2: $\Omega \rightarrow \Omega$, deforming images I_1 and I_2, respectively. The deformed images are then often compared in the mid-space through a cost function such as $\|I_1 \circ T_1 - I_2 \circ T_2\|_2^2$, and the output is eventually computed as $T{=}T_2 \circ T_1^{-1}$. The mid-space cost function is by definition invariant with respect to the ordering of the images.

With no additional constraints, the dimension of the mid-space registration problem (solving for T_1 and T_2) is twice as big as the standard asymmetric problem (solving for T). Also, the mid-space can drift arbitrarily far away from the native spaces of the images due to large changes in T_1 and T_2, for instance through combination with a transformation h, as $T_1 \bigcirc h$ and $T_2 \bigcirc h$, which decreases the mid-space cost function without changing the final $T{=}T_2 \circ h \circ h^{-1} \circ T_1^{-1}{=}T_2 \circ T_1^{-1}$. An example of this phenomenon is the situation where the optimization algorithm modifies T_1 and T_2 in order to shrink the regions where the two deformed images do not match, resulting in a decrease in the mid-space cost function, without necessarily changing the end result, T. To avoid these issues, additional constraints are often employed to keep the mid-space "in between" the native spaces. For instance, the two transformations may be forced to have opposite-sign displacement fields, as $T_1(x) = x + u(x)$ and $T_2(x) = x - u(x)$, resulting in the constraint $T_1(x) + T_2(x) = 2x$ (or similarly $T_1^{-1}(x) + T_2^{-1}(x) = 2x$) [7, 8, 12-14]. This reduces the degrees of freedom and to some extent prevents the mid-space drift, however, at the expense of limiting our ability to model all possible transformations T. An extreme example of this limitation would be the 2D case with the true transformation T being a 180° rotation about the origin, i.e. $T(x) = -x$, where no T_1 and T_2 will simultaneously satisfy both $T_1(x) + T_2(x) = 2x$ and $T_2(x) = T \bigcirc T_1(x)$. For

large deformations, opposite-sign velocity fields [9, 10, 15] and geodesic averaging are used to preserve the properties of the transformations [5, 6, 16]. Since there is no unique way to define the mid-space, the registration results can depend on the choice of the constraints imposed on T_1 and T_2.

Mid-space pairwise registration can also be performed by constructing an unbiased atlas from two images [10, 16, 17]. In atlas construction, the observed images are assumed to be instances generated from an atlas image with some geometrical and intensity variation. Therefore, the problem boils down to finding an atlas, $A{:}\Omega \rightarrow \mathbb{R}$, and regular transformations T_1^{-1} and T_2^{-1} that take the atlas from the mid-space to the native spaces of the two images, in such a way that the deformed versions of the atlas resemble the observed images. Using the SSD metric, the data term for such an optimization is the sum of two (asymmetric [18, 19]) subject-atlas distance terms, as in:[1]

$$\hat{T}_1, \hat{T}_2, \hat{A} = \underset{T_1, T_2, A}{argmin} \left[\int_\Omega \left(I_1(x) - A \circ T_1^{-1}(x) \right)^2 \mathrm{d}x + \int_\Omega \left(I_2(z) - A \circ T_2^{-1}(z) \right)^2 \mathrm{d}z \right]. \quad (1)$$

Comparing the images to the atlas in the physically meaningful native image spaces complies with the generative model assumption that the image is generated as a deformed version of the atlas (not vice versa), and that the Gaussian noise is added to the deformed atlas [18, 19]. The changes of variables $x = T_1(y)$ and $z = T_2(y)$ leads to:

$$\underset{T_1, T_2, A}{argmin} \int_\Omega \left[(I_1 \circ T_1(y) - A(y))^2 J_1(y) + (I_2 \circ T_2(y) - A(y))^2 J_2(y) \right] \mathrm{d}y, \quad (2)$$

where $J_1(y) \coloneqq \det \partial T_1(y)$ and $J_2(y) \coloneqq \det \partial T_2(y)$ are the Jacobian determinants of the two transformations. The $\hat{A}(y)$ minimizing the cost function is derived as [18]:

$$\hat{A}(y) = \frac{J_1(y)\, I_1 \circ T_1(y) + J_2(y)\, I_2 \circ T_2(y)}{J_1(y) + J_2(y)}. \quad (3)$$

In an explicit-atlas scheme, the transformations and the atlas can be iteratively computed from Eq. (1) and Eq. (3) [17]. However, the atlas can indeed be eliminated in Eq. (2) by substituting $A(y)$ with $\hat{A}(y)$, leading to an implicit-atlas data term [10]:

$$\hat{T}_1, \hat{T}_2 = \underset{T_1, T_2}{argmin} \int_\Omega \frac{(I_1 \circ T_1(y) - I_2 \circ T_2(y))^2}{J_1^{-1}(y) + J_2^{-1}(y)} \mathrm{d}y. \quad (4)$$

[1] Regularization terms such as the Tikhonov integrals $\int_\Omega \|\nabla T_1(x) - \mathbb{I}\|_F^2 \mathrm{d}x$ and $\int_\Omega \|\nabla T_2(x) - \mathbb{I}\|_F^2 \mathrm{d}x$ are also typically included in the cost function to keep the transformations meaningful and penalize excessive distortion. In this section, however, we focus only on the data term. The derivation of Eq. (4) is not impacted by the regularization terms, as they do not depend on A. Please note that anti-drift constraints are needed in addition to the regularization terms.

2.2 Independence from the Mid-Space

Equation (4) is an optimization over both T_1 and T_2, which define the mid-space. Even so, further simplification reveals that the two transformations are redundant. The change of variables $y{=}T_1^{-1}(x)$, with $\mathrm{d}y{=}\mathrm{d}x/J_1\circ T_1^{-1}(x)$, results in:

$$\hat{T}_1,\hat{T}_2{=}\underset{T_1,T_2}{argmin}\int_\Omega \frac{\left(I_1(x)-I_2\circ T_2\circ T_1^{-1}(x)\right)^2}{1+\frac{J_1\circ T_1^{-1}(x)}{J_2\circ T_1^{-1}(x)}}\mathrm{d}x. \quad (5)$$

Recall that the output transformation T is computed as $T(x){=}T_2\circ T_1^{-1}(x)$, the Jacobian determinant of which is $J(x):=det\,\partial T(x){=}J_2\circ T_1^{-1}(x)/J_1\circ T_1^{-1}(x)$. It now becomes clear that the above integral is, remarkably, only a function of T, and that the optimization can be written independently of the individual T_1 and T_2, as:

$$\begin{aligned}\hat{T}&{=}\underset{T}{argmin}D(I_1,I_2,T),\\ D(I_1,I_2,T)&:=\int_\Omega\left(I_1(x)-I_2\circ T(x)\right)^2\frac{J(x)}{1+J(x)}\mathrm{d}x.\end{aligned} \quad (6)$$

Thus, we can minimize this cost-function data term directly with respect to T, as opposed to the previous methods that optimize their cost functions with respect to both T_1 and T_2, conditioned to constraints that prevent the mid-space drift.

With $D(I_1, I_2, T)$ being independent of T_1 and T_2, the mid-space disappears, eliminating the problem of the mid-space drift as well. We do not need to enforce any anti-drift constraints anymore, hence not biasing the space of possible transformations T by the particular choice of such constraints. This is all while keeping the degrees of freedom of the optimization half of that of the unconstrained problem of solving for both T_1 and T_2. In addition, no transformation needs to be inverted to compute T, as opposed to most existing mid-space approaches that need to invert T_1 to compute $T{=}T_2\circ T_1^{-1}$. These advantages are especially valuable for displacement-field parameterized transformations, inverting which is a difficult and inexact task. Lastly, one can verify the expected symmetry of the proposed data term, i.e. $D(I_1, I_2, T) = D(I_2, I_1, T^{-1})$. Note that this symmetry holds only in the continuous domain. In the discrete case, where one image is resampled and the other is not, discretization artifacts produce a bias [19-21].

Equation (6) might seem like a non-uniform integral in the native space of I_1. However, this cost function originates from Eq. (1), which is the sum of two integrals taken uniformly in the native spaces of images, and non-uniformly only in the abstract mid-space. Therefore, the pitfalls associated with non-uniform integration in native spaces [11] are not expected to arise. We subsequently showed that Eq. (1) can be written independently of not only the atlas (Eq. (4) [10]), but also the mid-space itself (Eq. (6)).

2.3 Implementation

We implement the proposed registration method via the diffeomorphic demons scheme [22], and minimize $D(I_1, I_2, T)$ of Eq. (6) by gradient descent with line search. Similar to the demons algorithm, T is regularized by Gaussian blurring between each two descent iterations. We use a compositive scheme and update T by composing it with a transformation S, chosen to be the exponential of the update field. At each iteration, we fix T and J, and compute the variation of $D(I_1, I_2, T \bigcirc S)$ with respect to S, with S currently assumed to be the identity transformation. Then, to preserve the diffeomorphism, we initialize $S(x) = x - 2^{-M}\Delta\frac{\delta D}{\delta S}\big|_{S=\mathbb{I}}$ (for a large enough M), with Δ the step size, and compose it with itself ($S \leftarrow S \bigcirc S$) M times, before updating T as $T \leftarrow T \bigcirc S$ [22]. The variation is computed as follows (derivations omitted):

$$\frac{\delta}{\delta S} D(I_1, I_2, T \circ S)\Big|_{S=\mathbb{I}} = -\frac{2(I_1 - I_2 \circ T)J}{(1+J)^2}(\nabla I_1 + J\nabla(I_2 \circ T)) + \frac{2(I_1 - I_2 \circ T)^2 J}{(1+J)^3}\sum_{k=1}^{d} H^k.(C_{k,:})^{\mathrm{T}}, \quad (7)$$

where C is the cofactor matrix of ∂T with $C_{k,:}$ its k^{th} row, and H^k is the Hessian matrix of the k^{th} element of T. The notation (x) has been dropped for brevity. The last term of Eq. (7) involves the Hessian tensor of the deformation field, which can introduce large discretization error. In fact, the imprecision due to the discretization of the second derivative may outweigh the accuracy that this term is expected to bring about. In our experiments, ignoring this second-order term improved the optimization of Eq. (6).

3 Experimental Results

We tested the proposed deformable registration method on 2D slices of brain magnetic resonance images, using our in-house Matlab implementation of the diffeomorphic demons with the compositive scheme [22] (see Section 2.3). We compared our symmetric mid-space-independent registration method with the popular symmetrization approach that minimizes the average of the forward and backward cost functions [1-4], simplified in the form of $\int_\Omega (I_1(x) - I_2 \circ T(x))^2 \frac{1+J(x)}{2} \mathrm{d}x$, with $-(I_1 - I_2 \bigcirc T)(J\nabla I_1 + \nabla(I_2 \bigcirc T))$ being its compositive gradient. Each registration experiment consisted of 2000 gradient descent iterations, and was repeated with the demons regularization parameter taking a range of 22 different values.

3.1 Retrieval of Synthetic Deformations

In the first set of experiments, we compared the two algorithms on the mid-sagittal planes of 20 brain images taken from the publicly available OASIS database [23], which were pre-processed in FreeSurfer [24]. From each intensity-normalized and resampled volume (1-mm^3 isotropic voxel), the sagittal slice located four voxels to the right of the mid-sagittal plane was extracted, and resampled to the size 128×128 (Figure 1a). For each subject, two random deformation fields T_1^{synth} and T_2^{synth} were synthesized, spatially low-pass filtered, and applied to the sagittal slice, I, to produce two synthetically deformed images, $I_1 = I \circ T_1^{synth}$ and $I_2 = I \circ T_2^{synth}$ (Figure 1b,c), which were then registered with each other using both methods (Figure 1d,e). Ideally, we would expect to retrieve a transformation T

satisfying $T_1^{synth} \approx T_2^{synth} \circ T$. Accordingly, we computed the error $\int_\Omega \|T_1^{synth}(x) - T_2^{synth} \circ T(x)\|_2^2 \mathrm{d}x$, and for each subject and method, chose the best result (with the smallest error) across the experiments with different demons regularization values. Our mid-space-independent registration resulted in a lower error than the symmetrization method did in 14 out of the 20 subjects. On average, the error was 0.2% ± (SE) 0.2% lower for our method. We also ran the experiments in the reverse direction, and computed the inverse-consistency error, $\int_\Omega \|T_{\text{forward}} \circ T_{\text{backward}}(x) - x\|_2^2 \mathrm{d}x$, which was 4% ± 2% lower for our method than for the symmetrization method.

3.2 Cross-Subject Registration of Labeled Images

We performed a second set of experiments on a dataset of brain images with 37 neuroanatomical structures manually labeled [25]. We chose a fixed coronal slice maximizing the number of included distinct labels across the subjects (Figure 2). We randomly selected 40 pairs of subjects, and registered the chosen slices using the two methods. Although cross-sections of labels of 3D structures are not so precise for empirical validation, slice registration, being much faster than volumetric registration, allowed us to run many more experiments with a wide range of regularization.

We first considered 12 key subcortical regions: left/right amygdala, caudate, hippocampus, pallidum, putamen, and thalamus. As a similarity score for comparing the two methods, we computed in the union of these regions the portion of the voxels with matching labels between the two images. For each method and pair of subjects, we chose the maximum score achieved across different values of the demons regularization parameter. When the labels were compared in the native space of I_1, the two methods achieved on average similar scores (difference: 0.0% ± 0.2%). On the other hand, when the scores were computed in the native space of I_2 (by nearest-neighbor interpolation), the proposed method resulted in 0.10% ± 0.16% higher score than the symmetrization approach did.

In a different comparison, we computed the similarity score for each experiment by averaging the Dice's similarity coefficient across all of the labels. When the label overlaps were computed in the native space of I_1, the symmetrization approach produced a significant 0.7% ± 0.2% higher similarity score compared to the proposed method. When the scores were computed in the native space of I_2, however, the two algorithms performed similarly (0.0% ± 0.2%).

4 Conclusions

We have demonstrated for the first time that implicit-atlas pairwise registration is inherently independent of the mid-space, which led to deriving a new symmetric data term for deformable image registration. The independence of the cost function from the two image-to-atlas transformations alleviates the need for enforcing anti-drift constraints that can potentially bias the results. Our method is especially advantageous for the displacement-field transformation models, since inverting a velocity-field transformation is straightforward. We validated our method through experiments on two brain image datasets. Future work includes: a comprehensive evaluation of the proposed method on 3D labeled

data; investigating the practicality of the proposed framework for group-wise registration; and devising a suitable symmetric regularization scheme.

Acknowledgments

We would like to thank Dr. Ender Konukoglu for his valuable feedback on the evaluation of the method. Support for this research was provided in part by the National Institutes of Health (U24 RR021382, 8P41 EB015896, R01 EB006758, AG022381, R01 AG008122-22, R01 AG016495-11, RC1 AT005728-01, R01 NS052585-01, 1R21 NS072652-01, 1R01 NS070963, R01 NS083534, 1S10 RR023401, 1S10 RR019307, 1S10 RR023043, 5U01-MH093765, 1K25 EB013649, K25 CA181632). Additional support was provided by the Massachusetts Alzheimer's Disease Research Center (5P50 AG005134), BrightFocus Foundation (A2012333), the Autism & Dyslexia Project funded by the Ellison Medical Foundation, and the Gipuzkoako Foru Aldundia. BF has a financial interest in CorticoMetrics, a company whose medical pursuits focus on brain imaging and measurement technologies. BF's interests were reviewed and are managed by Massachusetts General Hospital and Partners HealthCare in accordance with their conflict of interest policies.

References

1. Christensen GE, Johnson HJ. Consistent image registration. IEEE Transactions on Medical Imaging. 2001; 20:568–582. [PubMed: 11465464]
2. Cachier P, Rey D. Symmetrization of the non-rigid registration problem using inversion-invariant energies: Application to multiple sclerosis. Proc. MICCAI. 2000:472–481.
3. Trouvé A, Younes L. Diffeomorphic matching problems in one dimension: Designing and minimizing matching functionals. Proc. ECCV. 2000:573–587.
4. Tagare H, Groisser D, Skrinjar O. Symmetric non-rigid registration: A geometric theory and some numerical techniques. J. Mathematical Imaging and Vision. 2009; 34:61–88.
5. Lorenzen P, Prastawa M, Davis B, Gerig G, Bullitt E, Joshi S. Multi-modal image set registration and atlas formation. Medical Image Analysis. 2006; 10:440–451. [PubMed: 15919231]
6. Avants B, Gee JC. Geodesic estimation for large deformation anatomical shape averaging and interpolation. Neuroimage. 2004; 23(Supplement 1):S139–S150. [PubMed: 15501083]
7. Yang D, Li H, Low D, Deasy J, Naqa I. A fast inverse consistent deformable image registration method based on symmetric optical flow computation. Phys Med Biol. 2008; 53
8. Noblet V, Heinrich C, Heitz F, Armspach J-P. An efficient incremental strategy for constrained groupwise registration based on symmetric pairwise registration. Pattern Recognition Letters. 2012; 33:283–290.
9. Lorenzi M, Ayache N, Frisoni GB, Pennec X. LCC-Demons: A robust and accurate symmetric diffeomorphic registration algorithm. Neuroimage. 2013; 81:470–483. [PubMed: 23685032]
10. Ashburner J, Ridgway GR. Symmetric diffeomorphic modelling of longitudinal structural MRI. Frontiers in Neuroscience. 2013; 6
11. Aganj I, Reuter M, Sabuncu MR, Fischl B. Avoiding symmetry-breaking spatial non-uniformity in deformable image registration via a quasi-volume-preserving constraint. Neuroimage. 2015; 106:238–251. [PubMed: 25449738]
12. Miller M, Banerjee A, Christensen G, Joshi S, Khaneja N, Grenander U, Matejic L. Statistical methods in computational anatomy. Stat Methods Med Res. 1997; 6:267–299. [PubMed: 9339500]
13. Studholme C, Cardenas V. A template free approach to volumetric spatial normalization of brain anatomy. Pattern Recognition Letters. 2004; 25:1191–1202.
14. Aljabar P, Bhatia KK, Murgasova M, Hajnal JV, et al. Assessment of brain growth in early childhood using deformation-based morphometry. Neuroimage. 2008; 39:348–358. [PubMed: 17919930]
15. Grenander U, Miller MI. Computational anatomy: an emerging discipline. Quarterly of Applied Mathematics. 1998; LVI:617–694.
16. Joshi S, Davis B, Jomier M, Gerig G. Unbiased diffeomorphic atlas construction for computational anatomy. Neuroimage. 2004; 23(Supplement 1):S151–S160. [PubMed: 15501084]

17. Hart GL, Zach C, Niethammer M. An optimal control approach for deformable registration. Proc. IEEE CVPR Workshops. 2009:9–16.
18. Ma J, Miller MI, Trouvé A, Younes L. Bayesian template estimation in computational anatomy. Neuroimage. 2008; 42:252–261. [PubMed: 18514544]
19. Sabuncu M, Yeo B, Van Leemput K, Vercauteren T, Golland P. Asymmetric image-template registration. Proc. MICCAI. 2009:565–573.
20. Aganj I, Yeo BTT, Sabuncu MR, Fischl B. On removing interpolation and resampling artifacts in rigid image registration. IEEE Trans. Image Process. 2013; 22:816–827. [PubMed: 23076044]
21. Reuter M, Rosas HD, Fischl B. Highly accurate inverse consistent registration: A robust approach. Neuroimage. 2010; 53:1181–1196. [PubMed: 20637289]
22. Vercauteren T, Pennec X, Perchant A, Ayache N. Diffeomorphic demons: Efficient non-parametric image registration. Neuroimage. 2009; 45:S61–S72. [PubMed: 19041946]
23. Marcus DS, Wang TH, Parker J, Csernansky JG, Morris JC, Buckner RL. Open Access Series of Imaging Studies (OASIS): Cross-sectional MRI data in young, middle aged, nondemented, and demented older adults. J. Cognitive Neuroscience. 2007; 19:1498–1507.
24. Fischl B. FreeSurfer. Neuroimage. 2012; 62:774–781. [PubMed: 22248573]
25. Fischl B, Salat DH, Busa E, Albert M, Dieterich M, Haselgrove C, van der KA, Killiany R, Kennedy D, Klaveness S, Montillo A, Makris N, Rosen B, Dale AM. Whole brain segmentation: automated labeling of neuroanatomical structures in the human brain. Neuron. 2002; 33:341–355. [PubMed: 11832223]

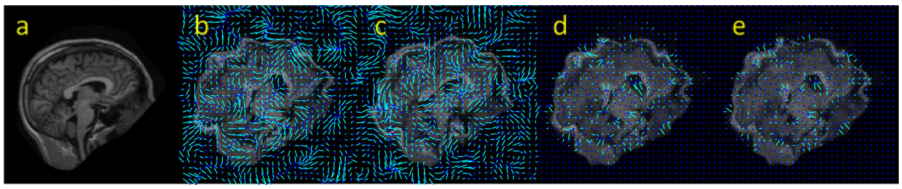

Figure 1.

The original image (a) was deformed by two synthetic random transformations (b,c). The deformed images were then registered with each other, resulting in deformation fields by the proposed (d) and the symmetrization (e) methods.

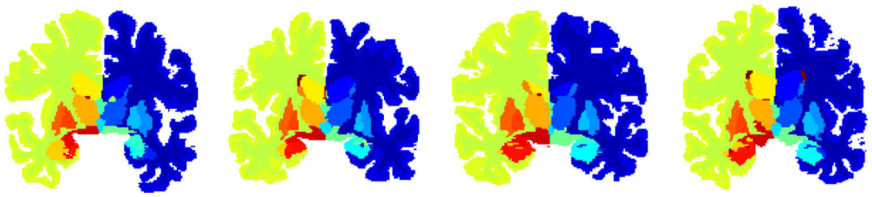

Figure 2.
Examples of the labeled coronal slices used in Section 3.2.